LA-UR-22-20222

Approved for public release; distribution is unlimited.

Title: Isolated Building Wake Experiment At Texas Tech University's Wind
             Engineering Research Field Lab

Author(s):   Nelson, Matthew Aaron; Duboc, Nicolas; Deshler, Mina Linsey; Conry, Patrick Tomas; Ortega,
                 Adrianna Kristyna; Linn, Rodman Ray; Gloeckler, Trey; Shah, Hussnain; Pol, Suhas

Intended for: Report

Issued: 2022-01-11

• Los Alamos
N A T I O N A L   L A B O R A T O R Y

Isolated Building Wake Experiment

At Texas Tech University's Wind Engineering Research Field Lab

Los Alamos
NATIONAL LABORATORY

Prepared by: Matthew Nelson[1], Nicolas Duboc[1], Mina Deshler[1], Patrick Conry[1], Adrianna Ortega[1], Rodman Linn[1], Trey Gloeckler[2], Hussnain Shah[2], and Suhas Pol[2]
[1]Los Alamos National Laboratory
[2]Texas Tech University

Derivative Classifier Review	
Reviewed and determined to be UNCLASSIFIED. This review does not constitute clearance for public release.	
Derivative Classifier	
Name/Z#/Org:	Matthew A. Nelson
Signature/Date:	1/3/2022
Derived from:	Earth Sciences DUSA

Contents

Figures

Tables

Contents

Abstract

Texas Tech University's (TTU's) Wind Engineering Research Field Lab (WERFL) building is an idealized rectangular building on the scale of a typical suburban house. It is surrounded almost entirely by unobstructed planes and is built on a turn table. WERFL is ideal for providing measurements of an idealized building under real-world conditions including atmospheric stability and variable relative wind angles. The intent of this data set is for verification and validation of computational fluid dynamics model simulations of flow around buildings. The primary focus of this dataset features 24 3D sonic anemometers (20 downwind and 4 upwind) and 10 2D sonic anemometers (9 downwind and 1 upwind) located in the immediate vicinity of the WERFL building. It also includes a variety of instruments intended to measure the ambient meteorological parameters and the undisturbed wind profile.

Acronyms and Abbreviations

Acronym	Definition
2D	two-dimensional
3D	three-dimensional
AGL	above ground level
ASL	atmospheric surface layer
CFD	computational fluid dynamics
H	building height
IBWE	Isolated Building Wake Experiment
L	building length
LANL	Los Alamos National Laboratory
PBL	planetary boundary layer
PBLH	planetary boundary-layer height
RMOL	reciprocal Monin-Obukhov length
TTU	Texas Tech University
W	building width
WERFL	Wind Engineering Research Field Lab

1 Introduction

The flow around an isolated building (or building-like object) has been studied continuously by a variety of researchers for more than a half century (e.g., Colmer 1971, Hansen et al. 1975, Hosker 1981, Snyder and Lawson 1994, Yassin 2009, Wang and Lam 2021). Much of the initial interest in the flow patterns that exist around buildings was due to the effects that buildings have on air quality in urban areas (Munn and Cole 1967, Drivas and Shair 1974, Hosker 1981, Huber 1991, Mavroidis et al. 1999, Monbureau et al. 2020). Later, others investigated how building wakes affect wind power generation (Leene 1992, Ge et al. 2021). The early efforts to provide detailed measurements of the flow around building were primarily performed using wind tunnel models (Hansen et al. 1975, Hunt et al. 1978, Hosker 1981, Peterka et al. 1985, Huber 1991, Snyder and Lawson 1994, Thomas and Williams 1999, Becker et al. 2002). As computational models have improved and the cost of performing computational fluid dynamics (CFD) simulations have decreased, the focus has transitioned from wind tunnel models to CFD simulations (Thomas and Williams 1999, Krajnovic and Davidson 2002, Barić 2010, Monbureau et al. 2020, Ge et al. 2021, Wang and Lam 2021). There have been relatively few field studies of flow around full-scale buildings in atmospheric surface layer (ASL) flow, due to the extreme cost and difficulty of executing such studies. Those full-scale field campaigns that have been performed typically have just a few measurement locations (Colmer 1971, Frost and Shahabi 1977).

Figure 1 shows a schematic of the flow structures that will develop around an idealized rectangular building under perpendicular flow. Upwind of the building the flow will separate from the surface and produce a rotor that circulates along the front face of the building and wraps around the sides of the building, also known as a horseshoe vortex. Recirculating regions will also develop downwind of the leading edges of the roof and sides of the building. The most prominent region with reversed flow will be found directly downwind of the building in the cavity zone. The majority of studies focus their attention on these highly complex regions immediately surrounding the building. The wake region, i.e., the region outside of the recirculating zones where the presence of the building is still evident and the flow transitions back to the ambient conditions (see Fig. 2), is of particular interest to distributed wind-energy production. Small-scale wind turbines are unlikely to be placed directly within the recirculating regions but it is typically desirable to minimize the distance from the wind turbines to the buildings that they power in order to minimize installation costs.

While wind-tunnel models and CFD simulations are useful and can provide a great deal of insight, they will always make some simplifying assumptions. The most obvious differences between the highly-idealized wind-tunnel models and/or CFD simulations and the real world are the steady-state in-flow profile and neutral thermal stability, which are employed in the majority of such studies with few exceptions (e.g., Kothari et al. 1979). Another common simplification is to have the ambient flow perfectly aligned with the sides of the building. Another important difference between the real world and these idealized studies is the undisturbed boundary layer. While many studies go to great lengths to replicate the characteristics of the ASL in their wind tunnel (Counihan 1969, Cook 1978, Cermak et al. 1995) or CFD simulation (Kosović and Curry 2000, Stoll 2020), there are physical constraints to the size of the wind tunnel and limits in computational resources that make it difficult to replicate the range of scales that can affect the flow and turbulence around a full-size building immersed within the planetary boundary layer (PBL). The height of the PBL (PBLH) will vary throughout the diurnal cycle from less than 100 m during the night to a few km during the day, depending on local conditions (Stull 1988). Limitations in measurement resolution and wind-tunnel size make it very difficult to replicate the ratio of building height to boundary layer height in the laboratory.

Introduction
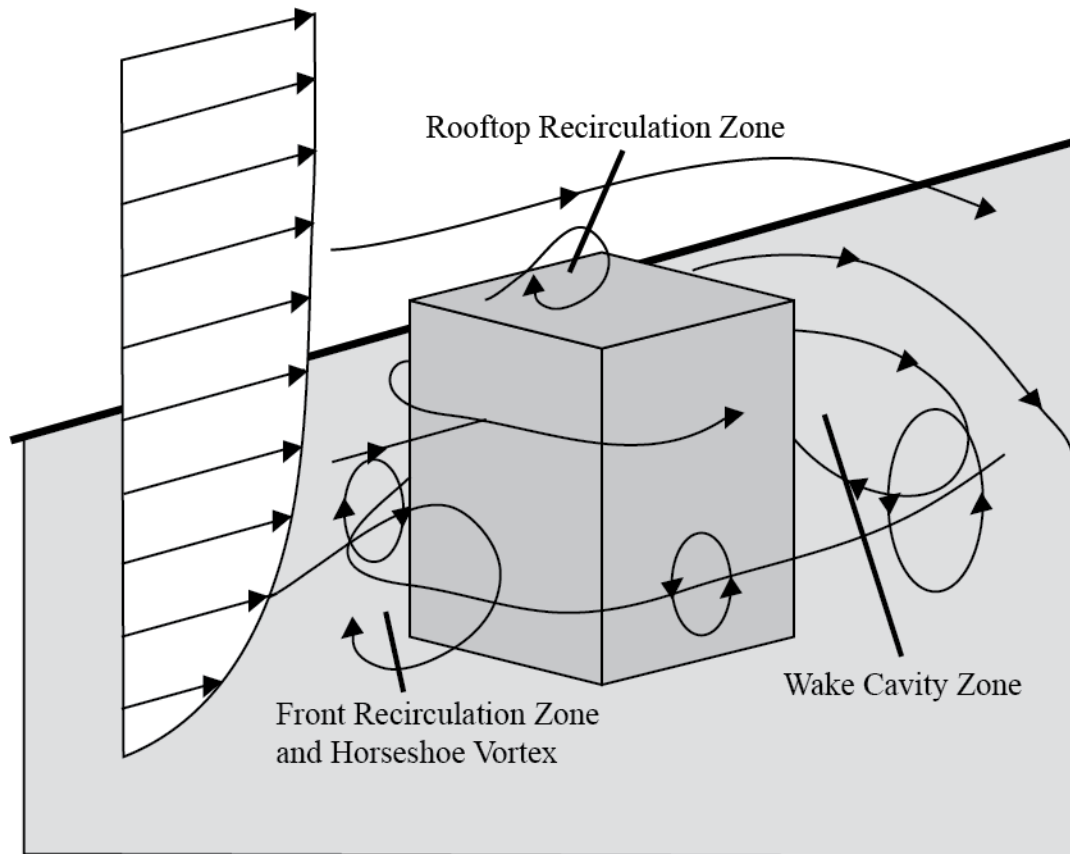
Figure 1. Schematic of the flow structures that develop around an idealized building under perpendicular winds
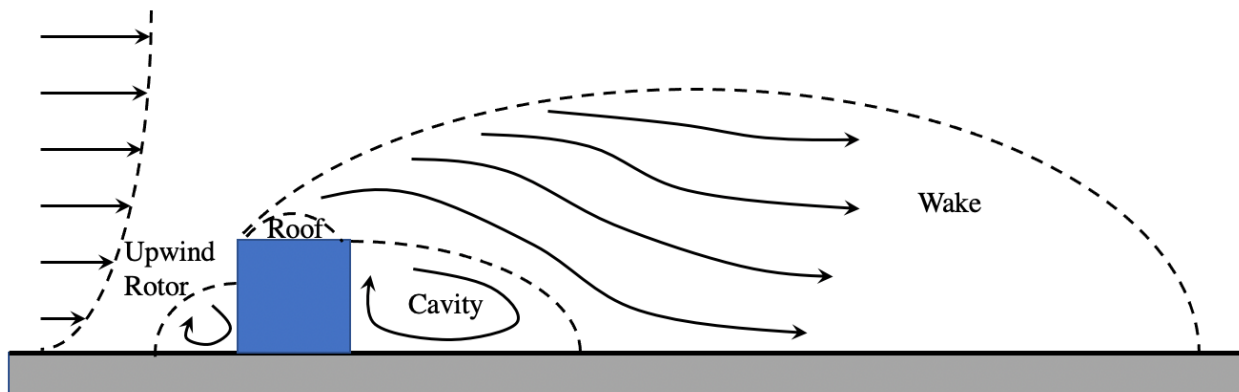
Figure 2. Schematic of flow regions that occur along the centerline of a building in boundary-layer flow

A building in the PBL will experience ambient conditions that are nearly always changing and cannot be controlled during the experiment: wind speed, wind direction, temperature, pressure, PBLH, turbulence, thermal stability, etc. These complicating factors can introduce flow phenomena that are difficult to replicate in laboratory or in simulations. Given the limitations of wind tunnel models and CFD simulations, full-scale field measurements are an important resource that can be used to validate the simplified methods. The primary focus of the Isolated Building Wake Experiment (IBWE) is to acquire

detailed measurements of the mean velocity and turbulence in the wake behind a simplified building under "real world" conditions, i.e., a full-scale building immersed in the atmosphere with all of the accompanying complications. The resulting dataset will provide a means of validating both high-fidelity CFD models and lower-order building wake models (Perera 1981, Kaplan and Dinar 1996, Brown et al. 2013).

1.1   The Wind Engineering Research Field Laboratory

Texas Tech University's Reese Technology Center is the home of the Wind Engineering Research Field Lab (WERFL) building. WERFL is a simple rectangular building that has been placed on a turn table to make it possible to reorient the building to test a variety of relative wind angles. The WERFL has approximately a 14-m width (W, width being defined as more normal to the wind than parallel), a 9-m length (L, aligned more with the wind than perpendicular), and a 4-m height (H). This is comparable to a typical suburban home in the United States. Due to the fact that the WERFL is located next to a decommissioned landing strip, it is located in near ideal conditions with very few obstructions in the vicinity of the building and no significant terrain that is likely to affect the flow. WERFL is located to the northwest of the Scaled Wind Farm Technology (SWiFT) site, which includes three utility-scale wind turbines. The historical wind roses for the months of operation (May-December) for the Isolated Building Wake Experiment (IBWE) are show in Figs. 4 and 5 (Kelley and Ennis 2016). Winds are predominantly from the south to southeast during the months of operation for IBWE.
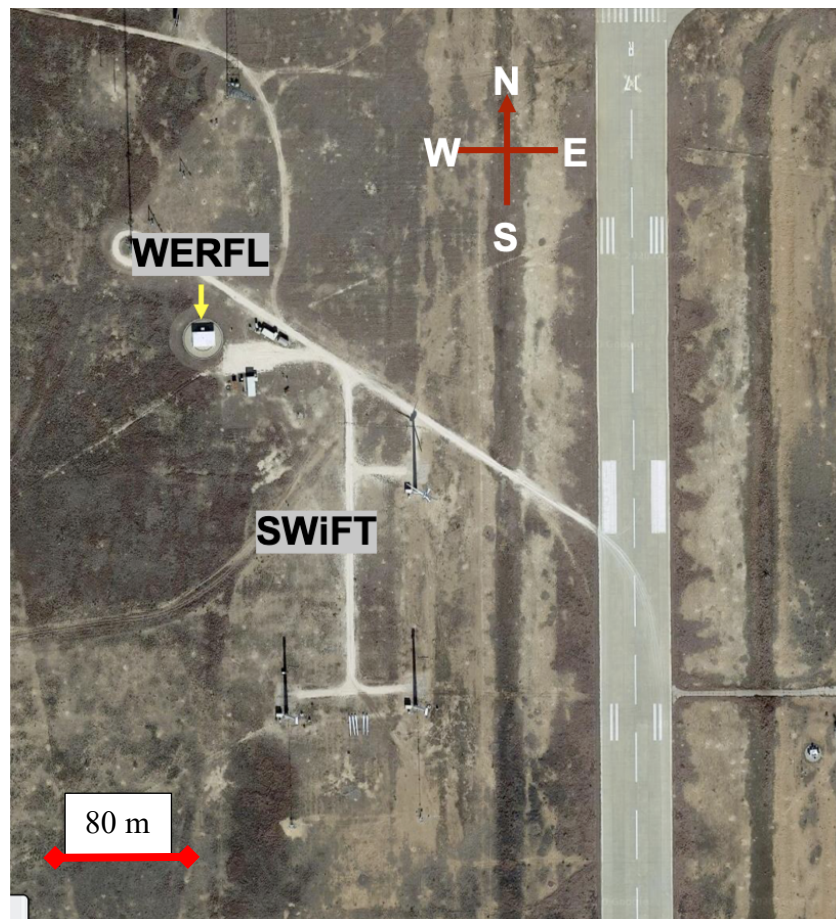
Figure 3. Location of the WERFL building relative to the SWiFT wind turbines. Aerial imagery courtesy of Google Earth

Introduction

(a) May

(b) June

(c) July
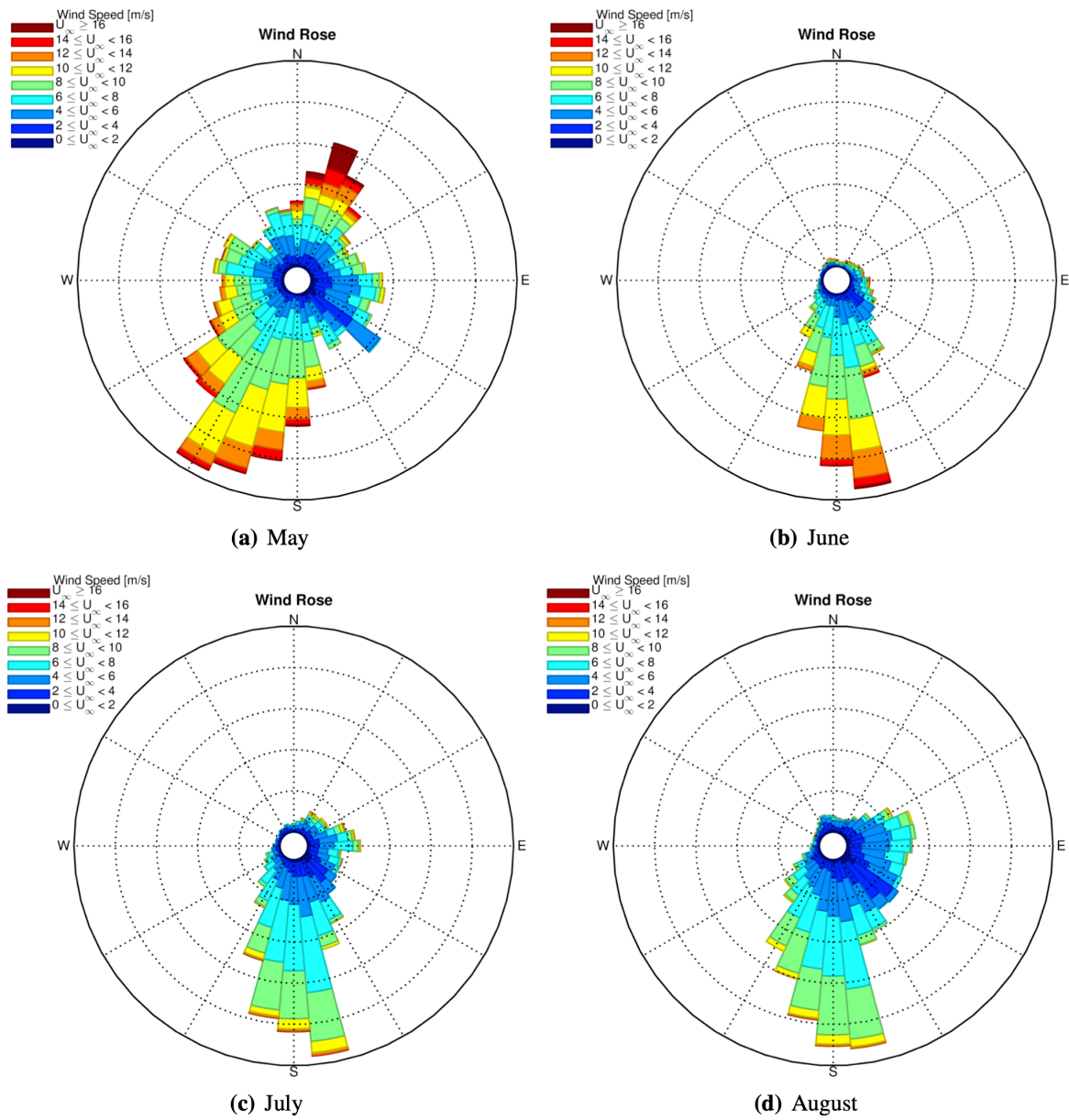
(d) August

Figure 4. Wind rose with wind speed intensity, May-August [Kelly and Ennis 2016, SAND2010216]

Isolated Building Wake Experiment
Los Alamos National Laboratory

(a) September   (b) October

(c) November   (d) December
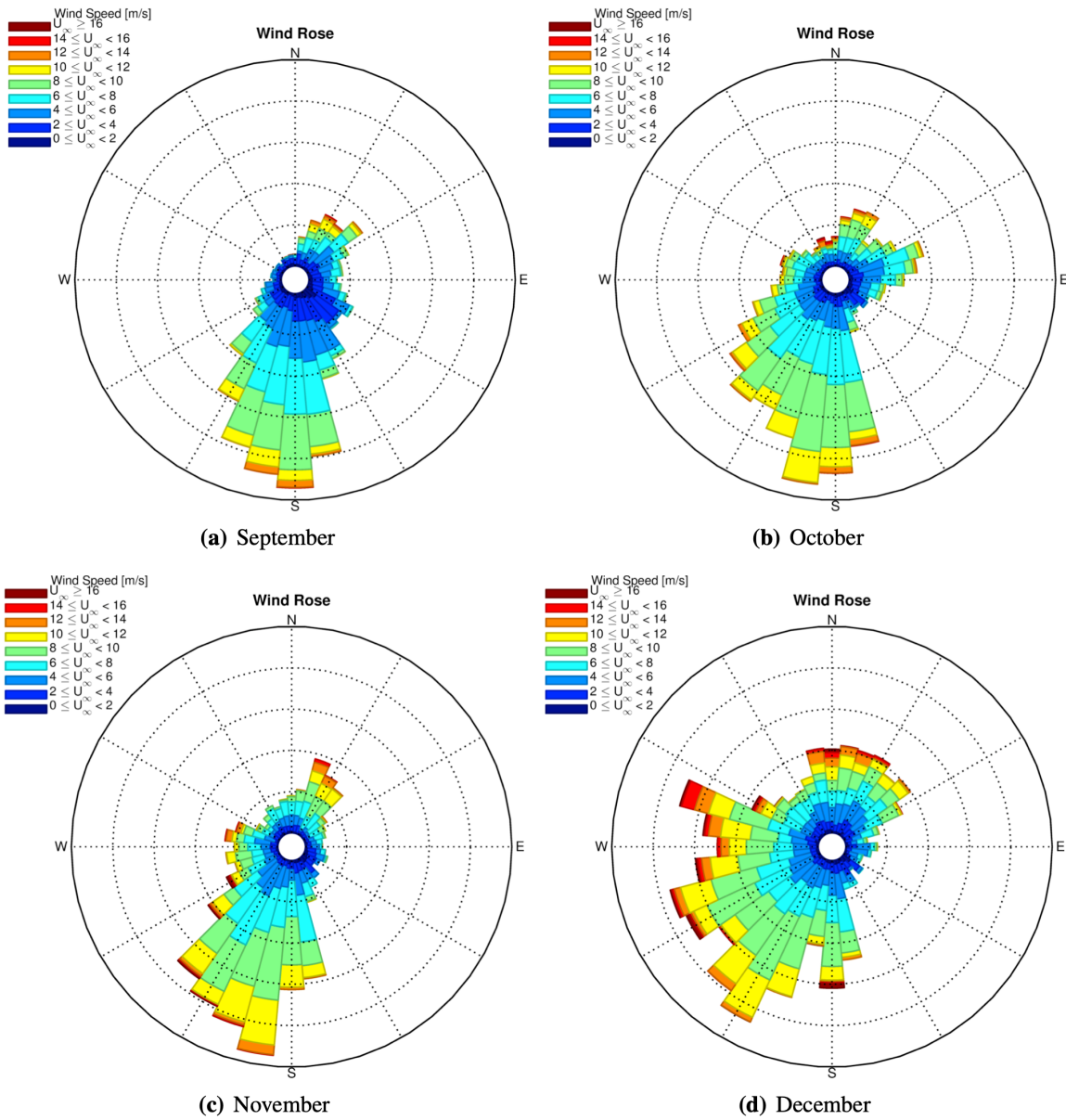
Figure 5. Wind rose with wind speed intensity, September-December [Kelly and Ennis 2016, SAND2010216]

2 Instrumentation

2.1 Sonic Anemometers

The primary focus of the IBWE is the high-frequency velocity and turbulence measurements using both 2D and 3D sonic anemometers located in the nominal wake of the WERFL building (i.e., to the north of the building, see Figs. 6 and 7). There are a total of 34 sonic anemometers that were deployed around the WERFL building, 29 nominally downwind of the building and 5 upwind to capture the undisturbed reference wind profile at the heights of the downwind measurements. The details of the positions of the sonic anemometers are found in Table 1. The rows of sonics are placed in increments of 3H downwind of the downwind wide face of the building. The center of the first two rows has a tower with sonics at 0.5H, H, 1.5H, and 2H AGL. The sonics in the 3H row are separated laterally in increments of H. The sonics in the 6H row are separated laterally by increments of 1.5H. the sonics in the 9H row are separated laterally by increments of 2H. The capabilities of the various types of sonic anemometers deployed in IBWE are presented in Table 2.

Figure 6. Locations of sonic anemometers deployed in the nominal wake (assuming southerly winds) at Texas Tech's Reese Technology Center. Aerial imagery courtesy of Google Earth

Data Correction

Table 1.   Description of sonic anemometers deployed around the WERFL turn table mounted building.

Station	Latitude	Longitude	Height	Sonic Type	Model
	Degrees	Degrees	Meters		
1	33.610193	-102.04999	2	3D	Metek USA-1
2	33.610301	-102.04995	2	3D	Metek USA-1
3	33.610301	-102.05020	2	3D	Metek USA-1
4	33.610193	-102.05016	2	3D	Metek USA-1
5	33.610409	-102.04999	2	3D	Metek USA-1
6	33.610409	-102.05016	2	3D	Metek USA-1
7	33.610193	-102.05012	2	3D	RM Young 81000V
8	33.610193	-102.05003	2	3D	RM Young 81000V
9	33.610301	-102.05001	2	3D	RM Young 81000V
10	33.610301	-102.05014	2	3D	RM Young 81000V
11	33.610409	-102.05007	2	3D	RM Young 81000V
12	33.610517	-102.05007	2	3D	RM Young 81000V
13	33.610193	-102.04995	2	2D	Gill WindSonic
14	33.610193	-102.04991	2	2D	Gill WindSonic
15	33.610301	-102.04982	2	2D	Gill WindSonic
16	33.610301	-102.04989	2	2D	Gill WindSonic
17	33.610301	-102.05026	2	2D	Gill WindSonic
18	33.610301	-102.05033	2	2D	Gill WindSonic
19	33.610193	-102.05024	2	2D	Gill WindSonic
20	33.610193	-102.05020	2	2D	Gill WindSonic
21	33.609702	-102.05029	2	2D	Gill WindSonic
22	33.610625	-102.05007	2	2D	Gill WindSonic
23	33.609702	-102.05032	2	3D	Campbell CSAT3
24	33.609702	-102.05032	4	3D	Campbell CSAT3
25	33.609702	-102.05032	6	3D	Campbell CSAT3
26	33.609702	-102.05032	8	3D	Campbell CSAT3
27	33.610193	-102.05007	2	3D	Campbell CSAT3
28	33.610193	-102.05007	4	3D	Campbell CSAT3
29	33.610193	-102.05007	6	3D	Campbell CSAT3
30	33.610193	-102.05007	8	3D	Campbell CSAT3
31	33.610301	-102.05007	2	3D	Campbell CSAT3
32	33.610301	-102.05007	4	3D	Campbell CSAT3
33	33.610301	-102.05007	6	3D	Campbell CSAT3
34	33.610301	-102.05007	8	3D	Campbell CSAT3

Figure 7. View from the southwest (near the upwind tower) showing the WERFL building and downwind sonic anemometers

Table 2. List of capabilities for each of the sonic anemometers as reported in user documentation:

Wind Speed

Model	Measuring Range	Measuring Resolution	Accuracy
	Meters/second		
Metek USA-1	0 – 50	0.01 m/s	0.1 m/s or 2%
RM Young 81000V	0 – 40	0.01 m/s	1 rms (0 – 30 m/s) 3 rms (30 – 40 m/s)
Gill WindSonic	0 – 60	0.01 m/s	2%
Campbell CSAT3	0 – 65.535	1 mm/s rms (horizontal) 0.5 mm/s rms (vertical)	8 cm/s (horizontal) 4 cm/s (vertical)

Wind Direction

Model	Measuring Range	Measuring Resolution	Accuracy
	Degrees	Degrees	
Metek USA-1	0 – 359	1	2° @ 5 m/s
RM Young 81000V	0.0 – 359.9	0.1	2 degrees (1 – 30 m/s) 5 degrees (30 – 40 m/s)
Gill WindSonic	0 – 359	1	3%
Campbell CSAT3	--	0.06 rms	0.7 degrees

Data Correction

2.2 Supplemental Instruments

In addition to sonic anemometers at 0.5H, H, 1.5H, and 2H, the near-surface temperature, relative humidity, surface temperature, and barometric pressure are each measured at the upwind tower at 2 m AGL (0.5H), i.e., collocated with Sonic 23 . The Vaisala HMP60 was placed in an Apogee TS-100 ventilated radiation shield. These instruments measure the ambient conditions in 1-minute averages. Profiling lidars measure the ambient wind profile. The details of the supplemental instruments deployed during IBWE are found in Table 3. Eight NRG Systems Spidar vertical profiling lidars have been deployed to the south (nominally upwind) of the the three wind turbines located to the southeast of WERFL building in Fig. 3 as part of the SWiFT experiment (Kelley and Ennis 2016). The westernmost of these lidars is located at 33.607275°, -102.049902°. The Spidars measure the upwind velocity profile from heights of 25 to 65 meters in five meter increments.

Table 3.   List of capabilities for each of the supplemental instruments as reported in user documentation:

Model	Measurement	Measuring Range	Accuracy
Vaisala HMP60	Near-surface Temperature	-40 – 60 degrees Celsius	0.6 degrees Celsius
Vaisala HMP60	Relative Humidity	0 – 100%	3% - 5% (0 - 90% RH) 5% - 7% (90 – 100% RH)
Apogee SB-100	Barometric Pressure	15 – 115 kPa	1.5%
Apogee SI-411	Surface Temperature	-45 – 80 degrees Celsius	0.2 degrees Celsius
NRG Systems Spidar	Wind Velocity Profile	Not Reported	0.4%

3 Data Correction

Some modifications to the data collected from a variety of 2D and 3D sonic anemometers were required due to unforeseen events during the time of data collection. These include adjustments to correct time stamps for all sonic anemometers and wind direction adjustments for anemometers located on the upwind and downwind towers.

Data from most stations (1-26) recorded data in UTC, stations located on the downwind tower (27, 28, 29, 30, 31, 32, 33, and 34) recorded data in local time. To remain consistent with the time stamps of the other stations these time stamps were adjusted to UTC +6 minutes due to a time drift discovered in the data.

3.1 Time Stamps

The sonic anemometer at Station 5 incurred time stamp errors beginning on August 14, when the station shut down and was unable to reconnect with the GPS. When it was restarted on August 25, it resumed from the last recorded time stamp, causing all of the time stamps to be shifted several days behind. In addition to this period of missing data, the station frequently shut off during the night, so the time stamps continued to be shifted backwards in time throughout the data-collecting period. Data from Station 5 was compared with uncompromised Stations (see Fig. 8) and the time stamps were adjusted until the predominant patterns of wind speed, wind direction, and temperature matched those found in the uncompromised (see Fig. 9).
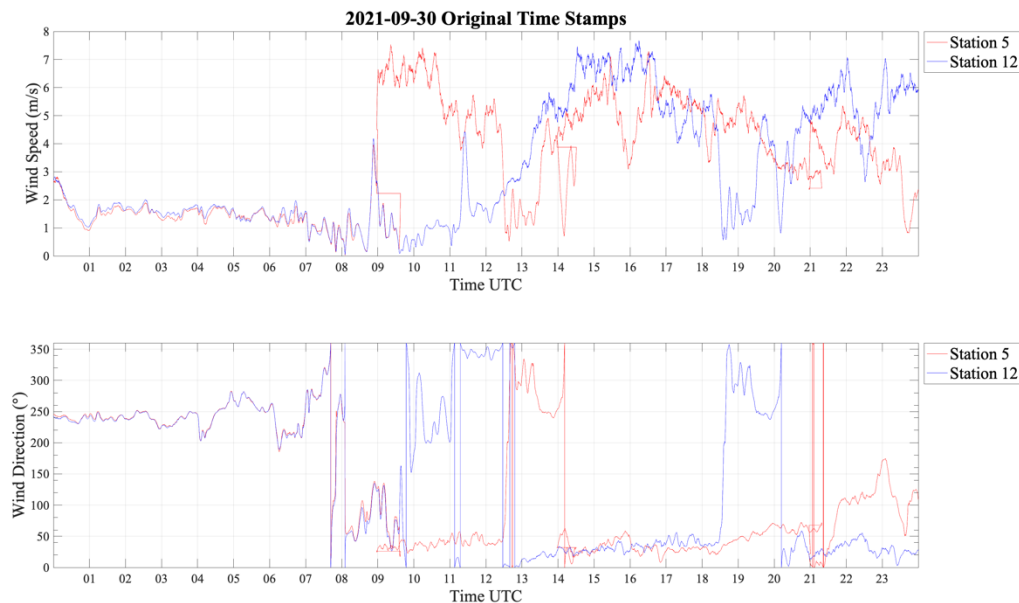

Figure 8. Comparison of averaged wind speed and wind direction for Station 5 and Station 12 before time stamp adjustment.
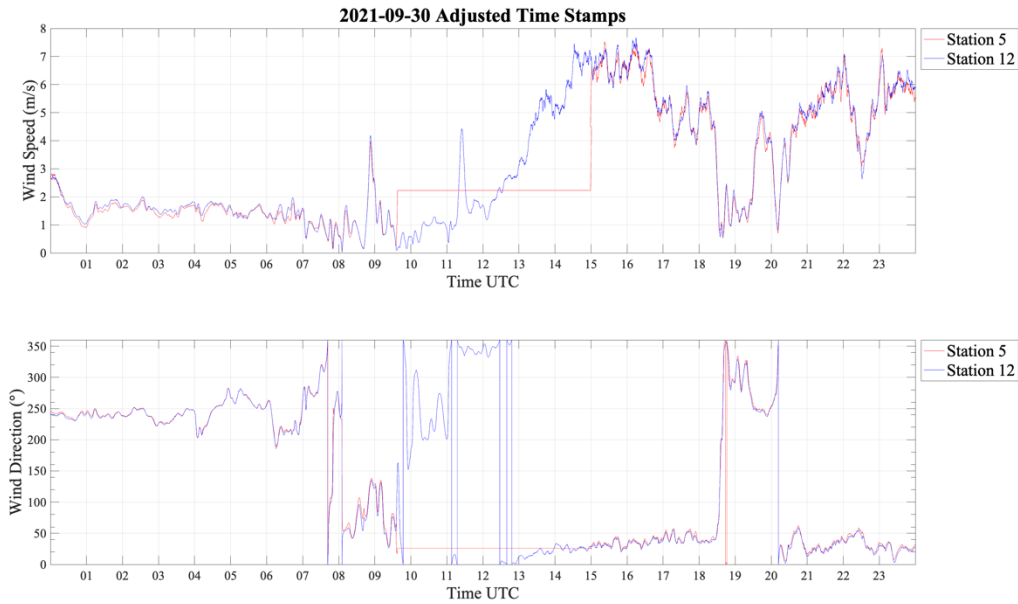
Data Correction

Figure 9. Comparison of averaged wind speed and wind direction for Station 5 and Station 12 after time stamp adjustment.

3.2　Wind Direction

Wind direction adjustments were made to all 12 Campbell sonic anemometers due to inconsistent alignment issues with true north. These adjustments were first made to the stations located on the upwind tower by comparing wind direction reported from Station 21, located 5 meters to the east of the tower at the same height as the lowest station. These included adjustments to stations 23, 24, 25, and 26. Given the location of the tower and Station 21 we determined a wind direction from 175-185 degrees should provide similar measurements from all five sensors. Station 21 data was split into 15 minute wind direction averages for every day until the appropriate wind direction was found. Figure 10 shows the sonic data from one of the upwind tower (Station 26) before and after it has been corrected. To avoid comparing meandering winds we ensured that the southerly component of the wind speed was at least 1m/s before calculating its wind direction. The data from the stations located on the upwind tower was then indexed at the same time step and the wind direction was calculated and compared. The average difference in wind direction (θ) was calculated for each sensor on the tower and applied to individual components of U and V. These were then applied to all measurements from each station on the tower:

$$Uc = U\cos(\theta) + V\sin(\theta)$$
$$Vc = -U\sin(\theta) + V\cos(\theta)$$

Where Uc and Vc are corrected wind speeds, U and V are original wind speeds, and θ is the difference of the wind angle of the tower and reference station in radians. A similar method was used for correcting the stations on the towers located 3 building heights (including Stations 27, 28, 29, and 30, e.g. Fig. 11,) and 6 building heights (including Stations 31, 32, 33, and 34, e.g.

Fig 12) from the downwind side of the structure. Instead of using the Station 21, however, the corrected data from Station 26 was used instead. In order to avoid capturing the wake from the structure and other smaller structures a predominantly westerly wind from 265-275 degrees was used to make these corrections. Similarly to the corrections made to the upwind tower, we ensured the westerly component of the wind was at least 1m/s before calculating its wind direction. Data was indexed at the appropriate time step to find the difference in wind direction and the same equations were applied to the entire data set. Given that Station 26 is located on the upwind side of the structure, comparisons between it and stations on the downwind towers are only made during days with predominantly westerly winds.
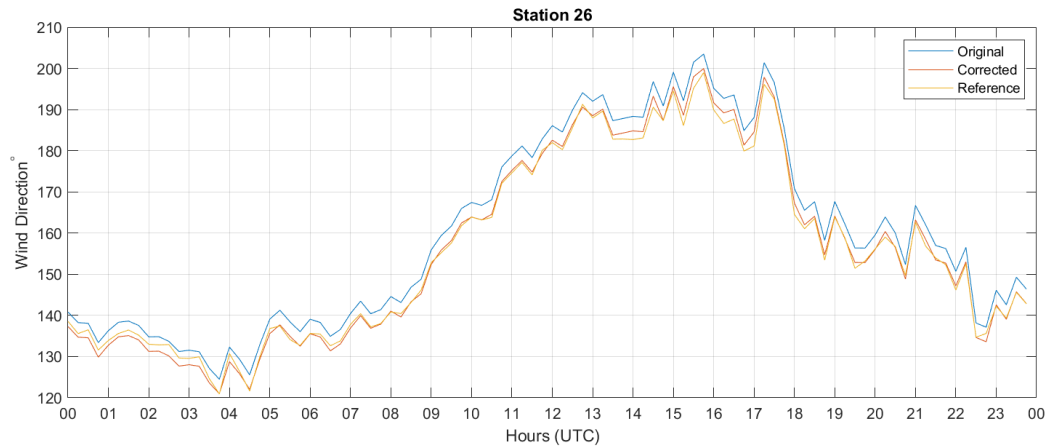
Figure 10. Comparison between original and corrected data for station 26 for July 17th, 2021. Reference is station 21

Figure 11. Comparison between original and corrected data for station 28 located on the 3H tower for July 18th, 2021. Reference is corrected data from station 26

Data Correction

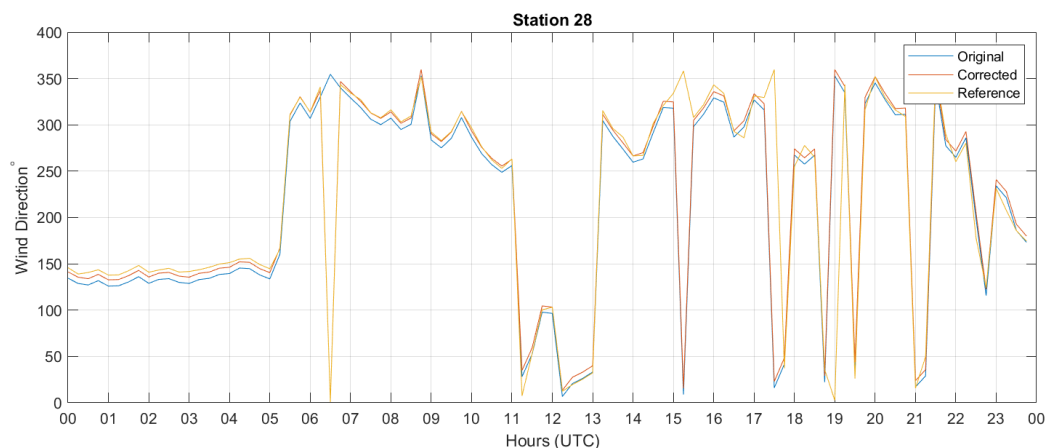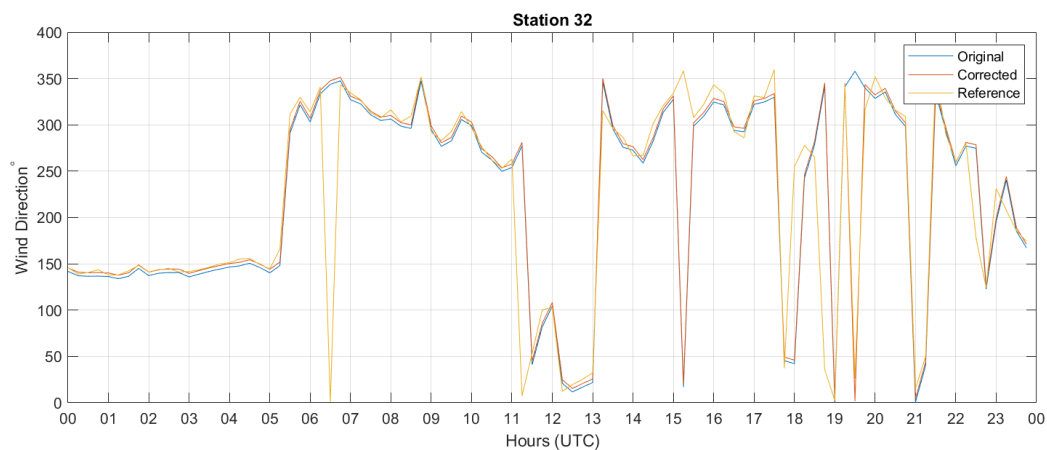Figure 12. Comparison between original and corrected data for station 32 located on the 6H tower for July 18th, 2021. Reference is corrected data from station

4 Example Data

In order to facilitate compatibility and ease of analysis, all of the data files are simple ASCII text CSV files, for which readers are readily available. Each data file includes a header that indicates the variable in the column and the units of the values. The location of the measurement is not included in the body of the file nor in the header line but the station number is included in the file name and the location of the sonic can be found by referring to Table 1. Velocity data is in a standard meteorlogical coordinates with positive U velocities blowing from west to east, positive V velocities blowing from south to north, and positive W velocities blowing up. All times are in UTC.

4.1   Time Series

These are examples of data captured on July 17, 2021. There was a large time period with nominally southerly winds on this day which transitioned from thermally stable to unstable conditions. Below are a series of figures (Figs. 13-19) depicting 10-minute averages of the wind direction, wind speed, temperature, friction velocity, turbulence kinetic energy, kinematic heat flux, and reciprocal Monin-Obukhov length from station 24. We have also included a vector plot (Fig. 20) including all active sonics at 17:00 UTC.
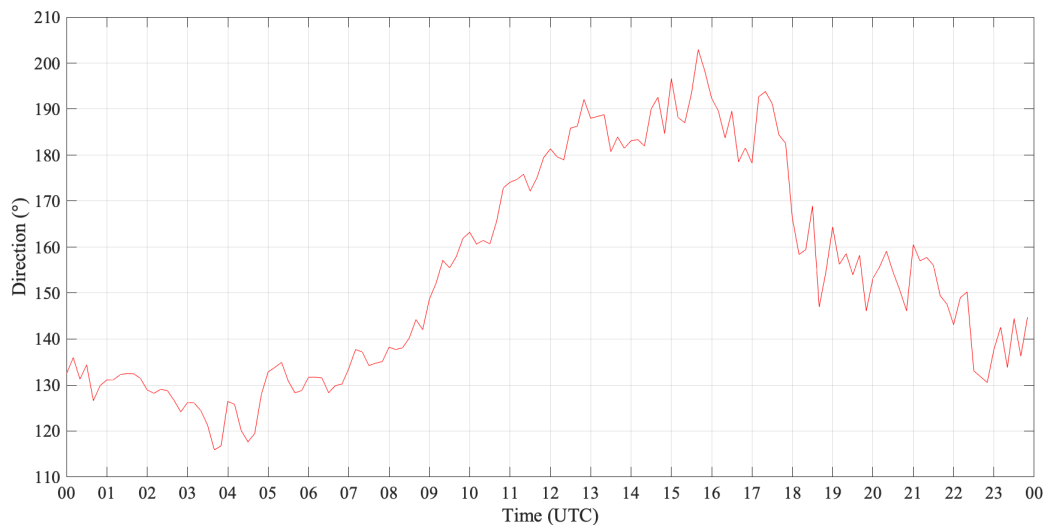
Figure 13. Wind direction measured by Sonic 24 for July 17, 2021 00:00 UTC to 23:59 UTC

Example Data
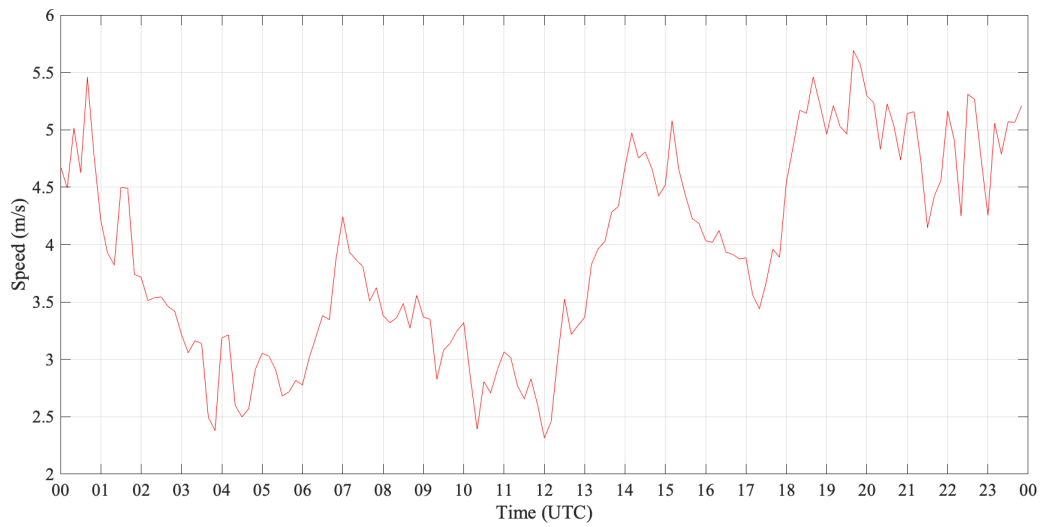
Figure 14. Vector wind wpeed measured by Sonic 24 for July 17, 2021 00:00 UTC to 23:59 UTC

Figure 15. Temperature measured by Sonic 24 for July 17, 2021 00:00 UTC to 23:59 UTC

Isolated Building Wake Experiment
Los Alamos National Laboratory

Figure 16. Friction velocity measured by Sonic 24 for July 17, 2021 00:00 UTC to 23:59 UTC

Figure 17. Turbulence kinetic energy measured by Sonic 24 for July 17, 2021 00:00 UTC to 23:59 UTC
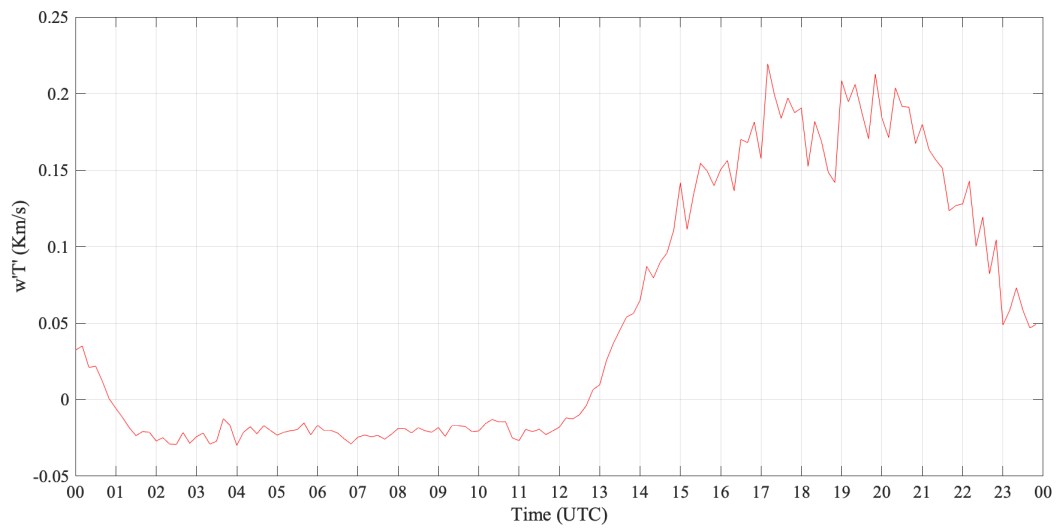
Example Data

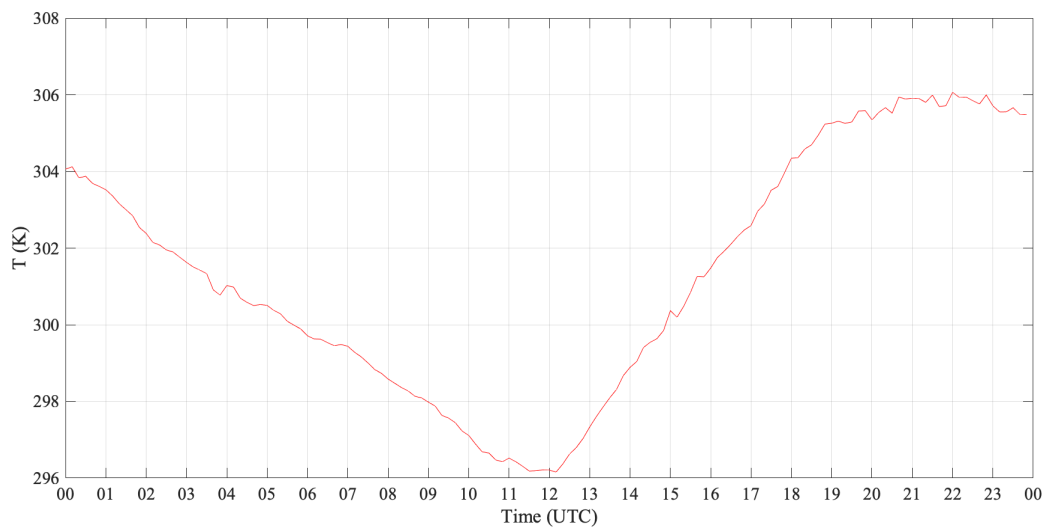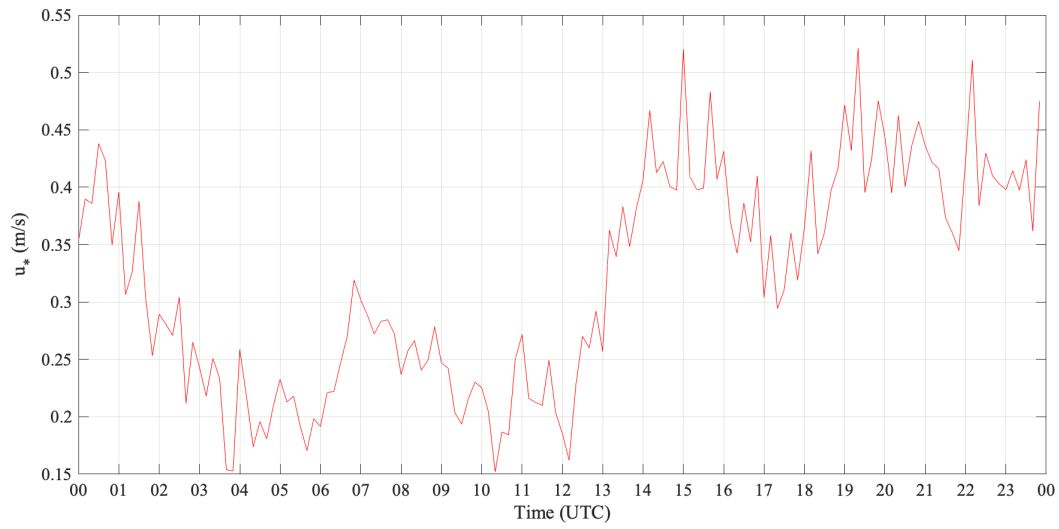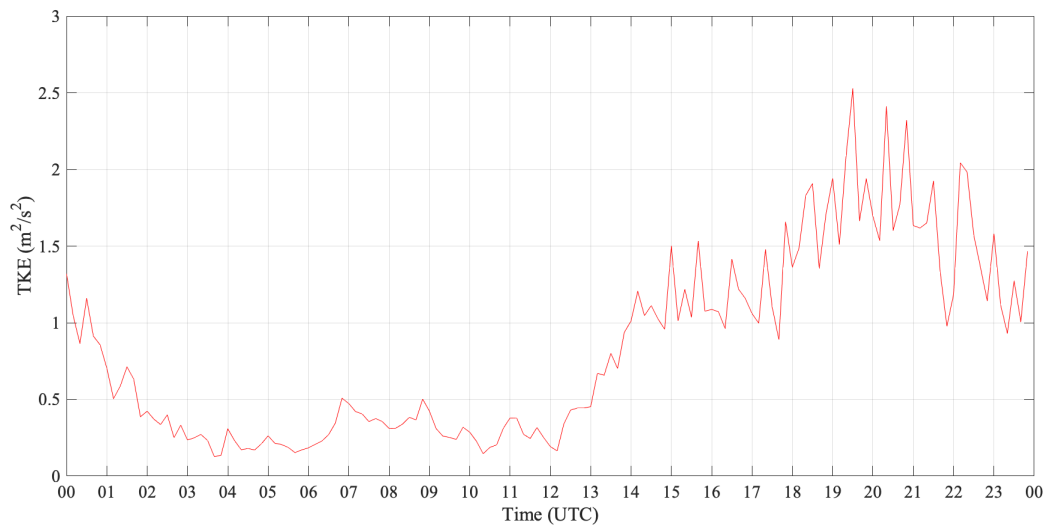Figure 18. Kinematic heat flux measured by Sonic 24 for July 17, 2021 00:00 UTC to 23:59 UTC
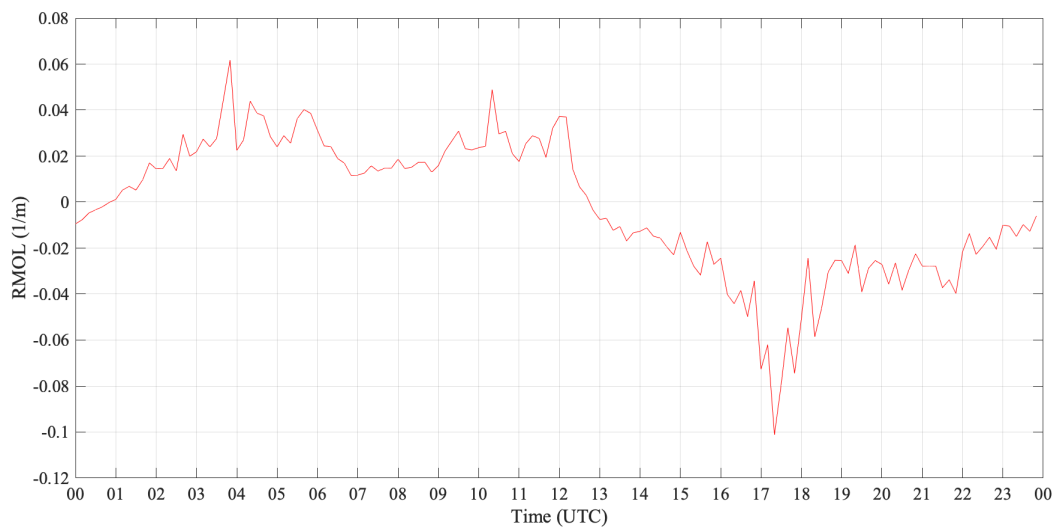
Figure 19. Reciprocal Monin-Obukhov length measured by Sonic 24 for July 17, 2021 00:00 UTC
to 23:59 UTC
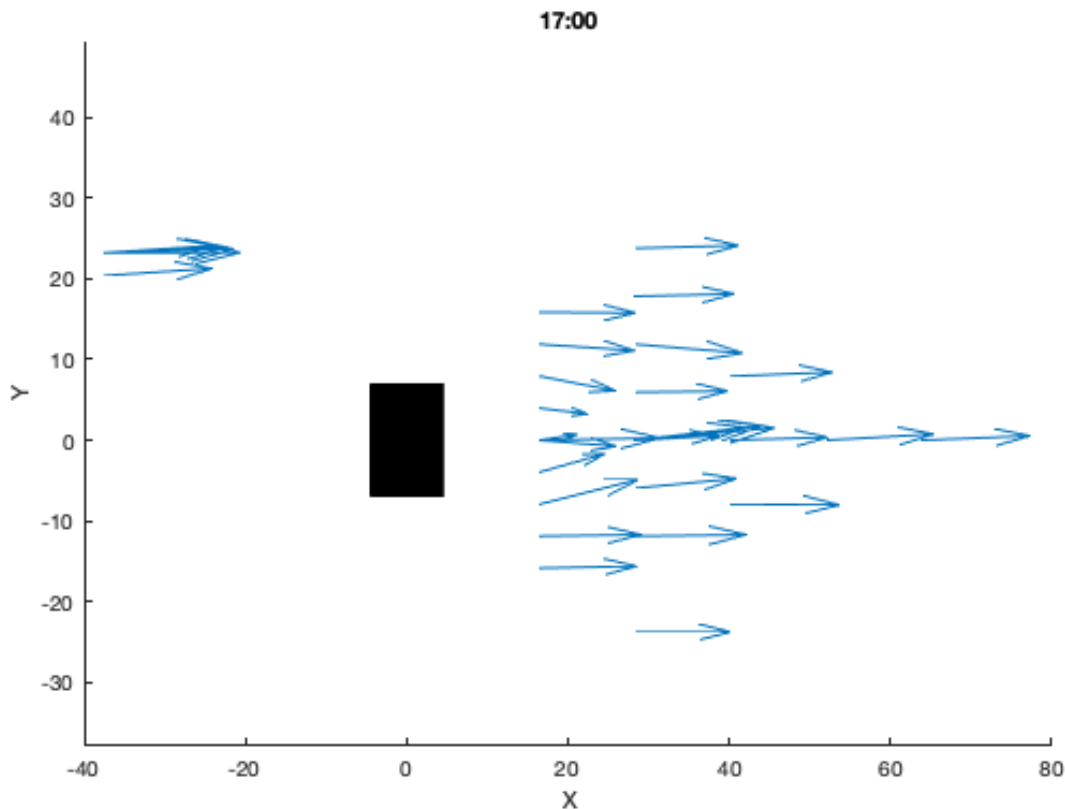
Figure 20. Example vectors averaged from data measured on 7/17/2021 from 17:00:00 to 17:09:59 UTC. The origin of the coordinate system is the centroid of the WERFL building with the positive X axis of the plot pointing to true north.

4.2   2D Sonic Data File Format

Below is a snipet of the data from Station 21 acquired on 7/17/2021 including the header:

```
Year,Month,Day,Hour,Minute,Second,U[m/s],V[m/s]
2021,07,17,00,00,00.19,-2.84,3.28
2021,07,17,00,00,00.24,-2.34,3.01
2021,07,17,00,00,00.49,-2.82,2.18
2021,07,17,00,00,00.74,-3.4,2.47
2021,07,17,00,00,01.21,-2.74,2.11
2021,07,17,00,00,01.46,-2.29,2.05
2021,07,17,00,00,01.71,-2.8,2.3
2021,07,17,00,00,01.96,-2.35,2.14
2021,07,17,00,00,02.17,-1.59,2.01
2021,07,17,00,00,02.42,-2.19,1.91
2021,07,17,00,00,02.67,-1.62,1.79
2021,07,17,00,00,02.93,-1.74,2.03
…
```

Example Data

4.3   3D Sonic Data File Format

Below is a snipet of the data from Station 8 acquired on 7/17/2021 including the header:

```
Year,Month,Day,Hour,Minute,Second,U[m/s],V[m/s],W[m/s],T[K]
2021,07,17,00,00,00.07,-4.21,1.68,-0.53,304.36
2021,07,17,00,00,00.17,-3.94,2.01,-0.28,304.46
2021,07,17,00,00,00.27,-3.92,2.25,0.08,304.27
2021,07,17,00,00,00.37,-3.55,2.57,0.29,304.22
2021,07,17,00,00,00.47,-3.25,2.34,0.24,304.32
2021,07,17,00,00,00.57,-3.14,2.09,0.31,304.47
2021,07,17,00,00,00.67,-2.96,2.29,0.34,304.38
2021,07,17,00,00,00.77,-3.43,2.28,-0.23,304.55
2021,07,17,00,00,00.87,-3.59,2.13,-0.45,304.45
2021,07,17,00,00,00.97,-3.68,2.41,-0.31,304.26
2021,07,17,00,00,01.06,-3.48,2.32,0.0,304.34
2021,07,17,00,00,01.16,-3.33,2.12,0.13,304.25
…
```

4.4   Supplemental Data File Format

In the supplemental upwind data file, "PTemp" is the temperature within the data logger box. "Press" is the barometric pressure measured within the data logger enclosure. "Temp" is the air temperature at approximately 2 meters AGL. "RH" is the relative humidity at approximately 2 meters AGL. "Stemp" is the surface temperature as measured by the infrared radiometer. Below is a snipet of the data acquired by the supplemental instruments deployed on the upwind tower on 7/17/2021 including the header:

```
Year,Month,Day,Hour,Minute,PTemp[C],Press[mbar],Temp[C],RH[%],STemp[C]
2021,7,17,0,0,33.78,887,30.49,50.16,31.03657
2021,7,17,0,1,33.76,887,30.53,50.28,31.06124
2021,7,17,0,2,33.74,887,30.56,49.92,31.06443
2021,7,17,0,3,33.72,887,30.59,50.43,31.04709
2021,7,17,0,4,33.7,887,30.59,49.93,30.93666
2021,7,17,0,5,33.68,887,30.59,50.25,30.78644
2021,7,17,0,6,33.66,887,30.53,49.94,30.65059
2021,7,17,0,7,33.64,887,30.49,50.48,30.64804
2021,7,17,0,8,33.62,887,30.44,49.88,30.69029
2021,7,17,0,9,33.6,887,30.43,51.15,30.82185
2021,7,17,0,10,33.58,887,30.47,50.96,30.95191
2021,7,17,0,11,33.56,887,30.51,50.52,30.81956
2021,7,17,0,12,33.54,887,30.51,51.44,30.94293
2021,7,17,0,13,33.52,887,30.59,51.13,30.81866
2021,7,17,0,14,33.5,887,30.61,50.39,30.49989
…
```

5 References

Barić, E., Džijan, I. and Kozmar, H., 2010. Numerical simulation of wind characteristics in the wake of a rectangular building submitted to realistic boundary layer conditions. *Transactions of FAMENA*, *34*(3), pp.1-10.

Becker, S., Lienhart, H. and Durst, F., 2002. Flow around three-dimensional obstacles in boundary layers. *Journal of Wind Engineering and Industrial Aerodynamics*, *90*(4-5), pp.265-279.

Brown, M.J., Gowardhan, A.A., Nelson, M.A., Williams, M.D. and Pardyjak, E.R., 2013. QUIC transport and dispersion modelling of two releases from the Joint Urban 2003 field experiment. *International journal of environment and pollution*, *52*(3-4), pp.263-287.

Cermak, J.E., Cochran, L.S. and Leflier, R.D., 1995. Wind-tunnel modelling of the atmospheric surface layer. *Journal of Wind Engineering and Industrial Aerodynamics*, *54*, pp.505-513.

Colmer, M.J., 1971. Some full-scale measurements of the flow in the wake of a hangar.

Cook, N.J., 1978. Wind-tunnel simulation of the adiabatic atmospheric boundary layer by roughness, barrier and mixing-device methods. *Journal of Wind Engineering and Industrial Aerodynamics*, *3*(2-3), pp.157-176.

Counihan, J., 1969. An improved method of simulating an atmospheric boundary layer in a wind tunnel. *Atmospheric Environment (1967)*, *3*(2), pp.197-214.

Drivas, P.J. and Shair, F.H., 1974. Probing the air flow within the wake downwind of a building by means of a tracer technique. *Atmospheric Environment (1967)*, *8*(11), pp.1165-1175.

Frost, W. and Shahabi, A.M., 1977. A field study of wind over a simulated block building, NASA Rep. *CR-2804*.

Ge, M., Gayme, D.F. and Meneveau, C., 2021. Large-eddy simulation of wind turbines immersed in the wake of a cube-shaped building. *Renewable Energy*, *163*, pp.1063-1077.

Hansen, A.C., Peterka, J.A. and Cermak, J.E., 1975. *Wind-tunnel measurements in the wake of a simple structure in a simulated atmospheric flow* (Doctoral dissertation, Colorado State University. Libraries).

Hosker Jr, R.P., 1981. *Methods for estimating wake flow and effluent dispersion near simple block-like buildings* (No. NOAA-TM-ERL-ARL-108). National Oceanic and Atmospheric Administration, Silver Spring, MD (USA). Air Resources Lab.

Huber, A.H., 1991. Wind tunnel and Gaussian plume modeling of building wake dispersion. *Atmospheric Environment. Part A. General Topics*, *25*(7), pp.1237-1249.

Hunt, J.C.R., Abell, C.J., Peterka, J.A. and Woo, H., 1978. Kinematical studies of the flows around free or surface-mounted obstacles; applying topology to flow visualization. *Journal of Fluid Mechanics*, *86*(1), pp.179-200

Kaplan, H. and Dinar, N., 1996. A Lagrangian dispersion model for calculating concentration distribution within a built-up domain. *Atmospheric Environment*, *30*(24), pp.4197-4207.

Kelley, C.L. and Ennis, B.L., 2016. *SWiFT site atmospheric characterization* (No. SAND-2016-0216). Sandia National Lab.(SNL-NM), Albuquerque, NM (United States).

Kosović, B. and Curry, J.A., 2000. A large eddy simulation study of a quasi-steady, stably stratified atmospheric boundary layer. *Journal of the atmospheric sciences*, *57*(8), pp.1052-1068.

Kothari, K.M., Peterka, J.A. and Meroney, R.N., 1979. *Stably stratified building wakes* (Doctoral dissertation, Colorado State University).

References

Krajnovic, S. and Davidson, L., 2002. Large-eddy simulation of the flow around a bluff body. *AIAA journal*, *40*(5), pp.927-936.

Leene, J.A., 1992. Building wake effects in complex situations. *Journal of Wind Engineering and Industrial Aerodynamics*, *44*(1-3), pp.2277-2287.

Mavroidis, I., Griffiths, R.F., Jones, C.D. and Biltoft, C.A., 1999. Experimental investigation of the residence of contaminants in the wake of an obstacle under different stability conditions. *Atmospheric Environment*, *33*(6), pp.939-949.

Monbureau, E.M., Heist, D.K., Perry, S.G. and Tang, W., 2020. Modeling lateral plume deflection in the wake of an elongated building. *Atmospheric Environment*, *234*, p.117608.

Munn, R.E. and Cole, A.F.W., 1967. Turbulence and diffusion in the wake of a building. *Atmospheric Environment (1967)*, *1*(1), pp.33-43.

Nozawa, K. and Tamura, T., 2002. Large eddy simulation of the flow around a low-rise building immersed in a rough-wall turbulent boundary layer. *Journal of Wind Engineering and Industrial Aerodynamics*, *90*(10), pp.1151-1162.

Perera, M.D.A.E.S., 1981. Shelter behind two-dimensional solid and porous fences. *Journal of Wind Engineering and Industrial Aerodynamics*, *8*(1-2), pp.93-104.

Peterka, J.A., Meroney, R.N. and Kothari, K.M., 1985. Wind flow patterns about buildings. *Journal of Wind Engineering and Industrial Aerodynamics*, *21*(1), pp.21-38.

Stoll, R., Gibbs, J.A., Salesky, S.T., Anderson, W. and Calaf, M., 2020. Large-eddy simulation of the atmospheric boundary layer. *Boundary-Layer Meteorology*, *177*(2), pp.541-581.

Stull, R.B., 1988. *An introduction to boundary layer meteorology* (Vol. 13). Springer Science & Business Media.

Snyder, W.H. and Lawson Jr, R.E., 1994. *Wind-tunnel measurements of flow fields in the vicinity of buildings* (No. CONF-940115-). American Meteorological Society, Boston, MA (United States).

Thomas, T.G. and Williams, J.J.R., 1999. Simulation of skewed turbulent flow past a surface mounted cube. *Journal of wind engineering and industrial aerodynamics*, *81*(1-3), pp.347-360.

Wang, F. and Lam, K.M., 2021. Wake of Elongated Low-Rise Building at Oblique Incidences. *Atmosphere*, *12*(12), p.1579.

Yassin, M.F., 2009. Numerical study of flow and gas diffusion in the near-wake behind an isolated building. *Advances in atmospheric sciences*, *26*(6), pp.1241-1252.